Journal of Energy Storage 72 (2023) 108085

Contents lists available at ScienceDirect

Journal of Energy Storage

journal homepage: www.elsevier.com/locate/est

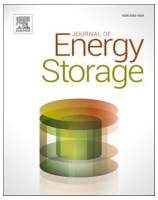

Research papers

Capacity and remaining useful life prediction for lithium-ion batteries based on sequence decomposition and a deep-learning network

Zili Wang [a], Yonglu Liu [a], Fen Wang [b,*], Hui Wang [a], Mei Su [a]

[a] School of Automation, Central South University, 410083 Changsha, China
[b] School of Civil Engineering, Central South University, 410083 Changsha, China

ARTICLE INFO

Keywords:
Deep learning network
Empirical mode decomposition
Lithium-ion battery
Remaining useful life prediction
Transformer

ABSTRACT

Lithium-ion batteries' remaining useful life (RUL) prediction is important for battery management systems, which are essential for ensuring the optimum performance and longevity of batteries used in different industries. However, accurate RUL prediction is challenging due to the complex degradation mechanism of the battery and actual noise operation conditions, particularly the capacity regeneration noise. To address this issue, this paper proposes a new method which combines a deep learning network with a sequence decomposition algorithm. Firstly, complementary ensemble empirical mode decomposition with adaptive noise algorithm is used to decompose the capacity fading sequence into a long-term residual and short-term fluctuations. This reduces the interference of the capacity regeneration phenomenon. Then, Transformer-based network is established to realize prediction for the separate components. This network architecture can handle the long-range dependency of the sequential data through its multi-head attention mechanism. The proposed method is validated through extensive experimentation using two publicly accessible battery datasets. The results show that the proposed method can achieve accurate and reliable prediction for both battery capacity and RUL, suggesting that this method can be a promising alternative for forecasting the performance and lifespan of batteries in practical applications.

1. Introduction

Lithium-ion batteries are widely used in electric vehicles and energy storage systems due to their high energy density, long lifespan, and low self-discharge rate [1]. As the number of charge-discharge cycles increases, the performance of the lithium-ion battery gradually deteriorates due to the cumulative impact of its internal and external environments. When the capacity reaches the end of life (EOL), the charge-discharge performance of the lithium-ion battery suffers significantly. Meanwhile, the battery will no longer meet the power consumption requirements of electrical equipment, making replacement necessary. As a result, the number of cycles between the starting point and the EOL, also known as the remaining useful life (RUL), is a crucial parameter for battery management [2]. Generally, the RUL prediction methods can be divided into the model-based and the data-driven methods.

The model-based RUL prediction method, such as the electrochemical model, the equivalent circuit model, and the empirical model, is based on the complex internal degradation mechanism of the battery [3]. Hu et al. [4] proposed an electrochemical mechanism-based moving average estimation model that takes into account accuracy, calculation strength, horizontal length, and fault tolerance. Based on a fractional-order equivalent circuit, Guha et al. [5] adopted the particle filter (PF) model to predict the RUL and the prediction results are more accurate than the conventional integer-order-based method. Lui et al. [6] proposed a prognostic method based on an empirical model that utilizes voltage and current analysis to predict the battery's RUL. However, because the chemical mechanisms inside the battery change over time, accurate prediction when using model-based methods is difficult [7]. In addition, model-based prediction methods are flawed due to their inherent limitations. The PF method is an instance where prediction accuracy decreases with particle degeneracy [8].

The data-driven method can predict the RUL of batteries based on feature information from their cycle data, without requiring prior knowledge of the battery's capacity fading mechanism [9]. The rapid development of machine learning technologies is accelerating the growth of data-driven methods for predicting battery RUL. M. Patil et al. [10] used the support vector machine (SVM) and critical feature method

* Corresponding author.
E-mail address: wfone1@csu.edu.cn (F. Wang).

https://doi.org/10.1016/j.est.2023.108085
Received 24 February 2023; Received in revised form 22 May 2023; Accepted 13 June 2023
Available online 5 July 2023

to accurately forecast RUL with improved speed and reduced error, based on cyclic data obtained from diverse operating conditions. Li et al. [11] utilized relevant vector machine and average entropy to accurately forecast the state of health (SOH) and RUL with multi-step advance prediction. Zhang et al. [12] demonstrated that the long short-term memory (LSTM) neural network outperforms the SVM, PF, and simple recurrent neural network (RNN) models for the prediction of long-term capacity. Robert R et al. [13] used gaussian process regression (GPR) to forecast the SOH and RUL. This approach exploited correlations among data from distinct batteries to produce accurate short-term and long-term predictions.

Although considerable results have been achieved in previous research, several areas still require improvement. For example, most methods process the original data directly without considering the capacitor regeneration (CR) phenomenon, which reduces the accuracy of RUL prediction [14]. The CR is a temporary increase in battery capacity caused primarily by the frequent switching between charging and discharging cycles. To improve the accuracy of RUL prediction, some researchers have used signal decomposition method to decompose the original data into stationary and fluctuating components. Empirical mode decomposition (EMD) is a time-frequency signal processing technique that decomposes signals into various components of different time scales without assuming a priori functional form. Zhou et al. [15] employed EMD to decompose the original capacity data into a residual component and intrinsic mode functions (IMFs). They then applied the autoregressive integrated moving average model (ARIMA) to predict the RUL. Based on EMD, Liu et al. [16] utilized LSTM and GPR to fit the IMFs and residual component, respectively. The results demonstrate that RUL prediction accuracy is enhanced when compared to single models.

RNN-based prediction networks (including RNN, GRU, and LSTM) model data in a cyclic manner, which results in extended training time and performance degradation due to long-term data dependence [17]. The attention mechanism (AM) has attracted significant attention in data-driven deep learning methods [18,19]. It can learn the weight distribution of original data independently and improve the feature representation ability of time series data. Wang et al. [20] proposed an AM-based bidirectional-LSTM (Bi-LSTM) method for RUL prediction. The AM was used to capture the most important features from a complete data sequence through attention weights. Experiment results showed that the AM-based method outperformed the original Bi-LSTM. However, since this AM-based neural network is still an RNN, its capacity to handle long time series remains restrictive.

Furthermore, since its introduction in 2017 [21], the Transformer, a deep learning network based entirely on the AM, has attracted wide attention. It addresses the limitations of RNNs, such as their inability to parallel compute information and model the periodicity of sequential data. By attending to different parts of the input sequence, the Transformer avoids the problem of circular learning, enabling it to capture relevant features more efficiently with less training data. Moreover, the model's architecture allows for parallel processing of the input sequence, which can speed up training and save time. Chen et al. [22] first built a RUL prediction model based on the Transformer, which outperformed the LSTM and GRU models in terms of both prediction performance and time cost. However, the denoising method used in this model to remove CR from the raw capacity data causes a reduction in RUL prediction accuracy.

Efficient prediction of battery RUL requires the selection of appropriate features, including physical parameters such as temperature, current, and voltage, as well as virtual parameters like capacity. While physical parameters are directly measurable, virtual parameters require representation by other physical parameters. In comparison with measured physical parameters, researchers consider battery capacity to be the definitive indicator of battery degradation [23], as changes in capacity directly reflect the degree of degradation of the battery during charge and discharge cycles. Capacity serves as a direct health factor for battery performance degradation and can predict the RUL of batteries. Accordingly, this paper adopts a capacity-based approach to achieve a satisfactory level of prediction accuracy.

The primary contributions of this paper are as follows:

1. The proposed method takes into account the CR phenomenon and employs the complete ensemble empirical mode decomposition with adaptive noise (CEEMDAN) algorithm to decompose the raw capacity sequence into short-term fluctuations and a long-term residual. The decomposition of the sequence enhances the accuracy of RUL prediction.
2. The Transformer model is utilized to model capacity fading data and achieve accurate prediction of the RUL. It can effectively capture useful features of the capacity sequences with less training data. This is accomplished by leveraging the multi-head AM of the Transformer, which also accelerates network learning and reduces training time.
3. The proposed method is derived, verified, and compared to several advanced methods on two publicly available battery aging datasets. The results demonstrate the effectiveness and superiority of this method.

The remaining sections of this paper are structured as follows: The proposed method for battery RUL prediction is described in Section 2. Section 3 provides details of the battery data used and the experimental setup for validating the proposed method. Section 4 verifies the effectiveness of the proposed method using different battery datasets. The conclusion is provided in Section 5.

2. Methods

2.1. Sequence decomposition

EMD can separate the CR from the battery capacity sequence and then divide the original sequence into a long-term residual and short-term fluctuations. On the other hand, it suffers from mode aliasing. Therefore, its improved version, the ensemble empirical mode decomposition (EEMD), is adopted [24] to solve this problem. The EEMD algorithm is described as follows:

1. Combine the initial signal $x[t]$ with Gaussian white noise $w^n[t]$ to acquire the reconstructed sequences $x^n[t]$:

$$x^n[t] = x[t] + w^n[t] \tag{1}$$

where $w^n[t]$ ($n = 1, 2 \ldots, N$) is different realization of the Gaussian white noise.

2. Use EMD to decompose the reconstructed signals $x^n[t]$ to obtain their IMFs $mn\ k[t]$, where $k = 1, 2 \ldots, K$ denotes the modes.
3. Average IMFs of corresponding modes k to obtain the EEMD decomposition modes $\overline{m}_k[t]$:

$$\overline{m}_k[t] = \frac{1}{N}\sum_{n=1}^{N} m_k^n[t] \tag{2}$$

However, if N is insufficient, the Gaussian white noise cannot be reduced to a negligible level, which can significantly impact the subsequent process analysis [25]. To address this issue, the CEEMDAN [26] algorithm is applied.

The white noise is added to the signal at each stage of the decomposition process. Then EMD is used to decompose the composite signal and to calculate the average of the first IMFs. The previous steps are repeated until the residual signal can no longer be decomposed. The termination conditions include two criteria: 1) the number of zero-crossings must be equal to or less than one deviation from the number of local extrema, and 2) the average of the upper and lower envelops is zero at any time. The decomposition process is explained in detail

through the following steps:

1. Add the Gaussian white noise $\varepsilon_0 w^n[t]$ to the original signal $x[t]$ to obtain new signals $x^n[t]$:

$$x^n[t] = x[t] + \varepsilon_0 w^n[t] \tag{3}$$

where ε_i ($i = 0, 1, 2 \ldots, I$) denotes the noise standard deviation of the Gaussian white noise.

2. Use EMD to decompose $x^n[t]$ and average the first modes to obtain the first CEEMDAN mode $\widetilde{m}_1[t]$:

$$\widetilde{m}_1[t] = \frac{1}{N}\sum_{n=1}^{N} E_1 x^n[t] \tag{4}$$

where $E_i(\cdot)$ represents the operator that generates the ith mode when the signal is decomposed by EMD.

3. Calculate the first residuals $r_1[t]$:

$$r_1[t] = x[t] - \widetilde{m}_1[t] \tag{5}$$

4. Add the special white noise $\varepsilon_1 E_1 w^n[t]$ to the residual $r_1[t]$, and decompose the composite signals by EMD to obtain the second CEEMDAN mode $\widetilde{m}_2[t]$:

$$\widetilde{m}_2 = \frac{1}{N}\sum_{n=1}^{N} E_1(r_1[t] + \varepsilon_1 E_1 w^n[t]) \tag{6}$$

5. Calculate the second residual $r_2[t]$:

$$r_2[t] = r_1[t] - \widetilde{m}_2[t] \tag{7}$$

6. Repeat steps 4 and 5 to obtain the kth mode $\widetilde{m}_k[t]$ and residual $r_k[t]$ (supposed the termination conditions are reached at the moment).

$$\widetilde{m}_k = \frac{1}{N}\sum_{n=1}^{N} E_1(r_{k-1}[t] + \varepsilon_{k-1} E_{k-1} w^n[t]) \tag{8}$$

$$r_k[t] = r_{k-1}[t] - \widetilde{m}_k[t] \tag{9}$$

Finally, the original signal can be represented as:

$$x[t] = \sum_{k=1}^{K} \widetilde{m}_k[t] + r_K[t] \tag{10}$$

2.2. Positional encoding

The Transformer model lacks a built-in mechanism for processing sequential data. To solve this problem, positional encoding is utilized to incorporate position information to the data sequence when processing time-series data [21]. In this paper, sine and cosine functions with varied frequencies are implemented:

$$PE(t, 2i) = sin\left(t/10000^{2i/d_m}\right) \tag{11}$$

$$PE(t, 2i+1) = cos\left(t/10000^{2i/d_m}\right) \tag{12}$$

where t and i represents the position and dimension of the input data, respectively. d_m denotes the length of the input data.

2.3. Transformer encoder

The Transformer model is an AM-based neural network. Unlike conventional RNNS, it uses self-AM to solve global dependency in sequential data, allowing it to learn complex patterns in dynamic time series. Self-AM is used to calculate the relevance of each element in the sequence to every other element, allowing the model to discover internal relationships within the time series [21].

To capture the mapping relationship between historical and future battery capacity data, this paper processes the time series data using a modified version of the original Google Transformer structure (encoder-decoder framework). The model consists of a stack of encoders, each with two sublayers: multi-head self-attention and feed-forward network. To enhance the model's performance, a residual connection [27] and layer normalization [28] are used between neighboring sublayers. The functions of these techniques are explained as follows:

1. The multi-head self-attention sublayer is used to learn the relationship between the input historical data and the output future data. Multiple self-AMs are used to calculate attention separately, and the results are added together. This mechanism expands the ability of the model to focus on different positions. Scaled dot-product attention is used and defined as follows:

$$Attention(\mathbf{Q}, \mathbf{K}, \mathbf{V}) = softmax\left(\frac{\mathbf{Q}\mathbf{K}^T}{\sqrt{d_h}}\right)\mathbf{V} \tag{13}$$

where $\boldsymbol{Q}$, $\boldsymbol{K}$, and $\boldsymbol{V}$ represent query vector, key vector, and value vector, respectively. d_h is used to adjust the product so that the inner product is not excessively large, thereby avoiding extremely small gradients [21].

The multi-head self-attention sublayer linearly maps $\boldsymbol{Q}$, $\boldsymbol{K}$, and $\boldsymbol{V}$ through the projection matrix before calculating $head_i$ and splicing the results. The calculation process of a single attention head is:

$$head_i = Attention\left(\mathbf{Q}\mathbf{W}_i^Q, \mathbf{K}\mathbf{W}_i^K, \mathbf{V}\mathbf{W}_i^V\right) \tag{14}$$

where projections matrices $\mathbf{W}_i^Q \in R^{d_m \times d_k}$, $\mathbf{W}_i^K \in R^{d_m \times d_k}$, and $\mathbf{W}_i^V \in R^{d_m \times d_v}$ ($i = 1, 2 \ldots, h$) are learnable parameters. Then, the output is:

$$MultiHead(h) = Concat(head_1, \cdots, head_h)\mathbf{W}^O \tag{15}$$

where projections matrix $\mathbf{W}^O \in R^{hd_v \times d_m}$ is obtained through training.

The weight distribution mechanism is used by the multi-head self-attention sublayer to identify input data, selectively ignore irrelevant data, and obtain essential information. Furthermore, because of the multi-head mechanism, the self-attention network can run in parallel, which speeds up the training process and saves time.

2. The feed forward sublayer is a fully connected network that has two linear and one ReLU nonlinear mappings. This layer is defined as follows:

$$FFN(z) = ReLU(\mathbf{W}_1 z + b_1)\mathbf{W}_2 + b_2 \tag{16}$$

where z represents the outputs of previous sublayer.

3. Residual connection is utilized to solve the problem of training multilayer networks. It makes the Transformer focus only on the current portion of the difference, which helps to avoid the vanishing gradient problem when the model depth is excessively large. Layer normalization converts the inputs of each layer of neurons to have the same mean and variance, improving the convergence of model training. Finally, the outputs of the multi-head self-attention sublayer Y_M and the feed forward sublayer Y_F can be represented as:

$$Y_M = Norm(MultiHead(h) + h) \tag{17}$$

$$Y_F = Norm(FFN(Y_M) + Y_M) \tag{18}$$

2.4. Transformer prediction

In order to predict future capacity, a full connection linear layer is used to map the relationship learned by the previous Transformer

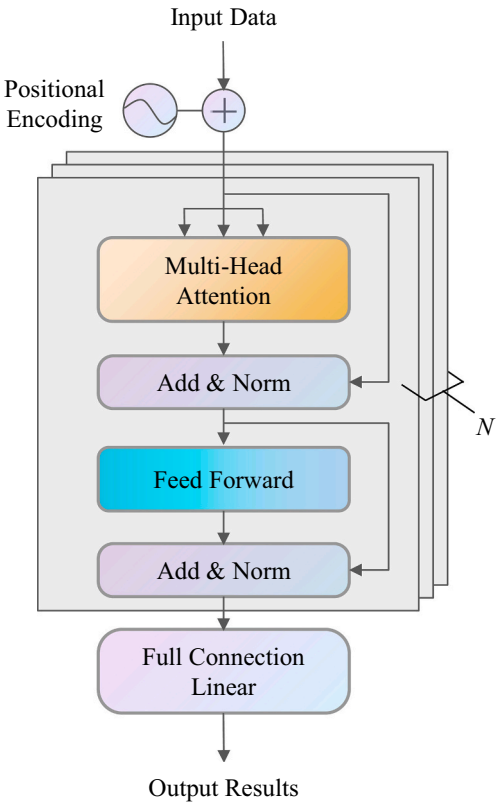

Fig. 1. Architecture of the Transformer network.

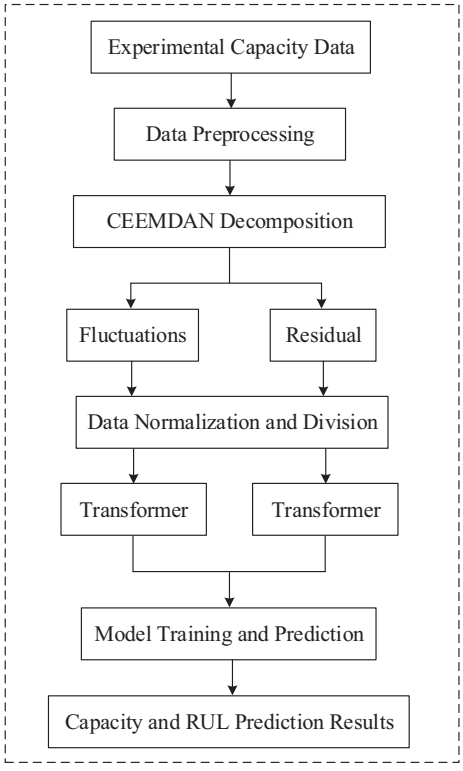

Fig. 2. Flow chart of the proposed combined method.

encoder and output the prediction result. It is expressed as:

$$y = f(\mathbf{W}_o e + b_o) \tag{19}$$

where e, $\boldsymbol{W}_o$ and b_o are input, weight, and bias of the linear layer. The architecture of the Transformer is shown in Fig. 1.

2.5. Combined method

A new combined lithium-ion battery RUL prediction method, namely CEEMDAN-Transformer, is proposed based on the advantages of each part. The CEEMDAN algorithm extracts component features from capacity fading sequences, which are then used by the Transformer model to accurately predict capacity and RUL. The flow chart of the proposed combined method is shown in Fig. 2. The specific steps are as follows:

Firstly, the experimental capacity data is preprocessed, such as outlier elimination and statistical analysis.

Then the clean data is decomposed into the short-term fluctuations and the long-term residual by using CEEMDAN.

Next, to lessen the impact of changes in the input data range, the data c needs to be normalized into a small scale by:

$$c^{'} = c/C_0 \tag{20}$$

where $c^{'} \in [0,1]$ represents the data after normalization and C_0 denotes the initial capacity of the battery.

After that, the normalized data is divided into the training data and testing data. Since there is no correlation between the training and testing data, the testing data is entirely novel for the Transformer model, ensuring prediction reliability.

Finally, the Transformer models are established to realize prediction for the separate components. The predicted capacity and RUL can be obtained by combining all the predicted components.

3. Experimental setup

3.1. Data description

This paper evaluates the effectiveness of the proposed method using NASA and CALCE battery datasets [29,30], which have been widely used in recent studies [30–42]. The battery degradation datasets are difficult to analyze due to their strong nonlinear and nonstationary characteristics.

The NASA datasets include four different types of Li-ion battery aging data, collected under three operating protocols: charge, discharge, and impedance measurements. Battery charge and discharge tests were performed at a constant temperature (24 °C). In the charge mode, the batteries were charged in the constant current (CC) mode at 1.5A until the voltage reached 4.2 V, at which point the mode switched to constant voltage (CV). In the discharging mode, the battery discharged at the CC mode until the voltage reached the preset value. Fig. 3a depicts the capacity change curves of NASA batteries as the cycle number increases. The terminal condition is that the battery capacity drops to 70 % of its original nominal capacity (from 2 Ah to 1.4 Ah). B0007 battery does not discharge to 1.4 Ah, so its normal operation range is 2 Ah to 1.5 Ah. B0005, B0006, and B0007 have a data length of 168, while B0018 has a data length of 132. Table 1 lists the dataset's specifications.

The CALCE datasets were collected at a constant temperature of 1 °C. In the charge mode, the battery operated in CC mode until the battery voltage reached 4.2 V. Then, the operation mode is changed to CV mode. In the discharge mode, the battery worked in the CC model to discharge capacity until the voltage dropped below 2.7 V. The terminal condition is identical to that of NASA, with the exception that the battery capacity ranges from 1.1 Ah to 0.77 Ah. Table 2 provides comprehensive details about the CALCE battery datasets. The capacity change curves of CALCE batteries are shown in Fig. 3b as the cycle number increases.

The datasets provided by NASA and CALCE comprise numerous

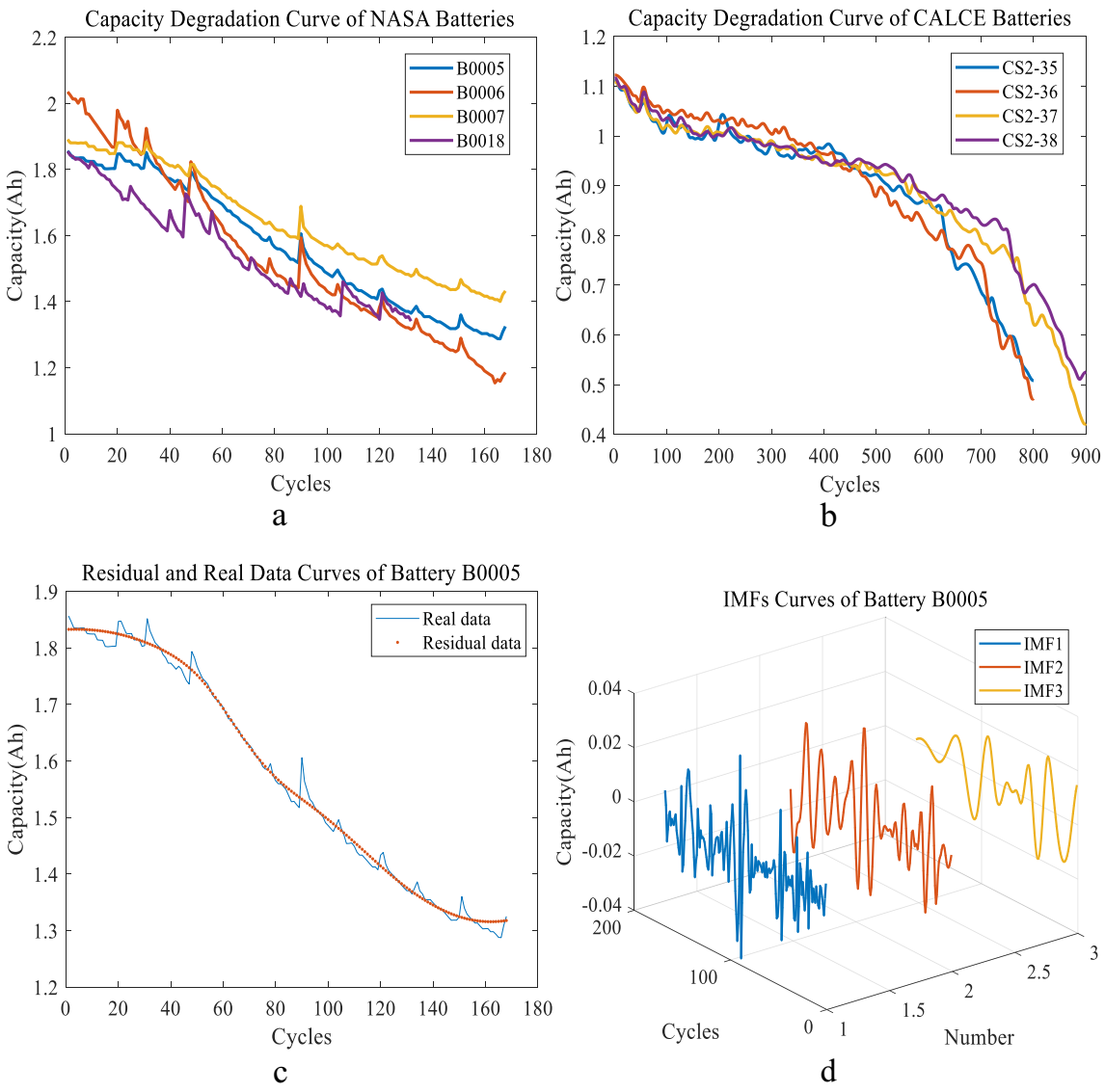

Fig. 3. Capacity degradation curves of batteries NASA and CALCE. a, NASA batteries. b, CALCE batteries. c, Residual and real data curves of battery B0005. d, IMFs (IMF1, IMF2, IMF3) curves of battery B0005.

Table 1
Specification of NASA datasets.

Type	Capacity (Ah)	Cutoff Voltage (V)	Discharge Current (A)	Temperature (°C)
B0005	2	2.7	2	24
B0006	2	2.5	2	24
B0007	2	2.2	2	24
B0018	2	2.5	2	24

Table 2
Specification of CALCE datasets.

Type	Capacity (Ah)	Cutoff Voltage (V)	Discharge Current (A)	Temperature (°C)
CS2_35	1.1	2.7	1.1	1
CS2_36	1.1	2.5	1.1	1
CS2_37	1.1	2.2	1.1	1
CS2_38	1.1	2.5	1.1	1

parameters, such as temperature, current, voltage and capacity. Temperature, voltage, and current can be utilized as indirect indicators of battery health, while capacity changes directly reflect the extent of battery degradation during charge and discharge cycles. With an increase in the number of cycles, the battery's capacity decreases and can be considered a crucial health factor for predicting the RUL of batteries based on battery performance degradation.

3.2. Decomposition of the datasets

The proposed method incorporates the CEEMDAN algorithm to extract the features of the raw capacity sequence. The capacity is extracted as the aging feature to describe the aging behavior of lithium-ion batteries. The NASA's B0005 capacity data is used as an example to

Table 3
Pearson correlation coefficient between residual and real data.

Type	Coefficient	Type	Coefficient
B0005	0.9972	CS2-35	0.9950
B0006	0.9930	CS2-36	0.9973
B0007	0.9970	CS2-37	0.9992
B0018	0.9879	CS2-38	0.9994

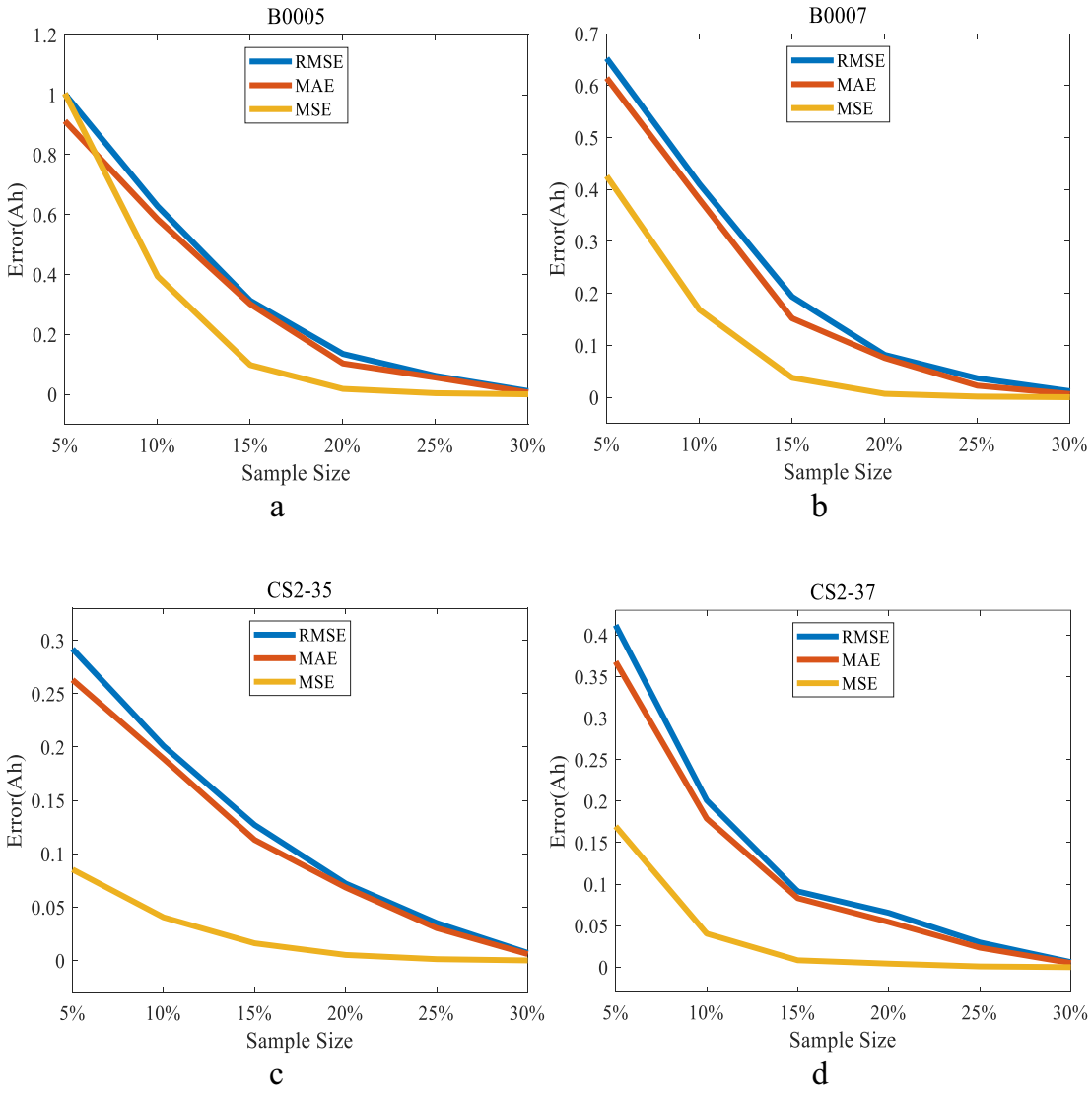

Fig. 4. Prediction errors with different training sample sizes (from 5 % to 30 %). a, B0005. b, B0007. c, CS2-35. d, CS2-37.

demonstrate the decompose mechanism. Using this method, the raw capacity data is decomposed into several IMFs and one residual sequence, as shown in Fig. 3.

The residual data curves in Fig. 3c demonstrate the strong agreement between the residual and real data, which represents the general trend of degradation. The Pearson correlation analysis method is employed to assess the association between the residual and raw sequences. Table 3 reports the correlation coefficients of the two public datasets. The findings of the correlation analysis reveal that each residual's Pearson correlation coefficient exceeds 0.98. This suggests that the residual can effectively reflect the battery's degradation trend while significantly mitigating the impact of CR. From Fig. 3d, it can be concluded that the IMFs are inconsistent with the degradation trend of the actual battery capacity data, indicating the CR phenomenon. Despite their small magnitude, IMFs will cause errors in the modeling process and RUL prediction if they are not considered [31]. The proposed CEEMDAN decomposition method effectively separates the short-term fluctuations from the global degradation trend of the experimental fading data. Then, the subsequent Transformer model can utilize separate short-term and long-term information to accurately predict the future capacity and RUL.

3.3. Evaluation criterion

In this paper, mean absolute percentage error (MAPE), mean absolute error (MAE), and root-mean-square-error (RMSE) are used to evaluate the performance of the proposed Transformer model.

$$MAPE = \frac{1}{n}\sum_{i=1}^{n}\left|\frac{y_{real}(i) - y_{pred}(i)}{y_{real}(i)}\right| \times 100\% \tag{21}$$

$$MAE = \frac{1}{n}\sum_{i=1}^{n}\left|y_{real}(i) - y_{pred}(i)\right| \tag{22}$$

$$RMSE = \sqrt{\frac{1}{n}\sum_{i=1}^{n}\left|y_{real}(i) - y_{pred}(i)\right|^2} \tag{23}$$

where n represents the number of cycles between the prediction starting point (ST) and the battery failure threshold. y_{real} and y_{pred} represent the real and predicted capacity data, respectively.

The metrics **Error** and **PError** are used to display the differences between real RUL and predicted RUL, and they are described below:

$$Error = \left|RUL_{real} - RUL_{pred}\right| \tag{24}$$

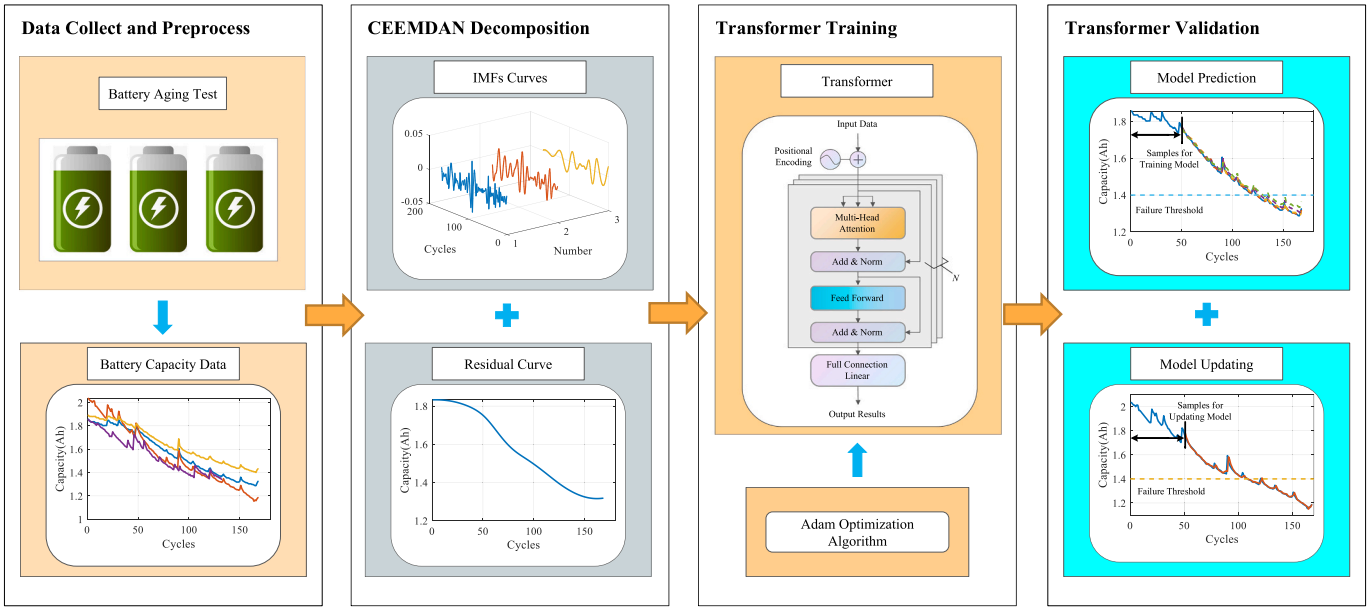

Fig. 5. Experimental flow of the proposed method.

$$PError = \frac{|RUL_{real} - RUL_{pred}|}{RUL_{real}} \times 100\% \tag{25}$$

where RUL_{real} and RUL_{pred} represent the real and predicted values, respectively.

3.4. Specifications of the model

There are six important parameters for the proposed Transformer model: learning rate (τ), depth (l) and hidden size (s), regularization for learning (λ), ratio of each task (α), and training sample size (m).The top five parameters are determined by grid search on the validation error: $\tau \in \{10^{-4}, 5\times10^{-4}, 10^{-3}, 5\times10^{-3}, 10^{-2}\}$, $l \in \{1,2,3,4\}$, $s \in \{8,16,32,64\}$, $\lambda \in \{10^{-6}, 10^{-5}, 10^{-4}, 10^{-3}\}$, and $\alpha \in (0,1]$. The iteration number is set to 500 epochs. The Adam algorithm is used to optimize the network training process, and the model training loss function is the mean square error (MSE), which is given by:

$$MSE = \frac{1}{n}\sum_{i=1}^{n}\left(y_{real}(i) - y_{pred}(i)\right)^2 \tag{26}$$

The training sample size m is determined by an iterative trial method, which is set to 30 % of the sequence length. To test the feature extraction and prediction performance of transformers under a small amount of training data. For this purpose, we used the capacity data from batteries B0005, B0007, CS2-35 and CS2-37 as the testing battery data. The training sample size m is selected from 5 % to 30 % [36]. Fig. 4 depicts the prediction errors with different proportions of training data. The results demonstrate that the prediction errors, including RMSE, MASE, and MSE, decrease as the proportion of training data increases. It's worth noting that the proposed model exhibits the highest precision when trained on a 30 % training set. As a result, the proposed model is trained using 30 % of the total degradation data.

3.5. Experimentation design

1. **Comparative experiments:** To verify the superiority of the proposed method's improvements, we conducted comparative experiments with LSTM and Transformer models using batteries B0005, B0007, CS235, and CS2-37.
2. **Model online validation:** A prediction program is carried out to verify the online prediction ability of the proposed method. Trained models are employed to predict the future capacity and RUL of batteries B0006, B0018, CS2-36, and CS2-38. The models are updated with 30 % measured battery capacity fading data without retraining. The experimental flow of the proposed method is depicted in Fig. 5.
3. **Time cost analysis:** An experiment is designed to show the computation performance of the Transformer model, using batteries B0005 and CS2-35. To provide a basis for comparison, RNN-based networks, including RNN, GRU, and LSTM, are used as reference targets.
4. **Comparison with other advanced methods:** In order to further validate its performance, we compared the predicted results of the proposed method, utilizing NASA and CALCE datasets, with those of other advanced methods in the existing literature.

4. Results and discussion

4.1. Comparative experiments

Tables 4 and 5 display the prediction results for batteries B0005 and B0007, respectively. In this case, PRUL denotes the predicted RUL. Fig. 6a and b depicts the estimated capacity degradation curves for battery B0005. The LSTM model's estimated capacity reached the EOL at the 131st cycle, which is six cycles larger than the actual RUL value.

Table 4
Prediction results of battery B0005.

Method	RMSE(Ah)	MAE(Ah)	MAPE	RUL	PRUL	Error	PError
LSTM	0.0262	0.0221	1.58 %	125	131	6	4.80 %
Transformer	0.0173	0.0145	1.01 %	125	128	3	2.40 %
CEEMDAN-LSTM	0.0129	0.0094	0.63 %	125	126	1	0.80 %
CEEMDAN-Transformer	**0.0109**	**0.0060**	**0.41 %**	125	**125**	**0**	**0**

Table 5
Prediction results of battery B0007.

Method	RMSE(Ah)	MAE(Ah)	MAPE	RUL	PRUL	Error	PError
LSTM	0.0256	0.0218	1.44 %	126	133	7	5.56 %
Transformer	0.0181	0.0154	1.00 %	126	131	5	3.97 %
CEEMDAN-LSTM	0.0175	0.0141	0.92 %	126	131	5	3.97 %
CEEMDAN-Transformer	**0.0116**	**0.0063**	**0.40 %**	**126**	**126**	**0**	**0**

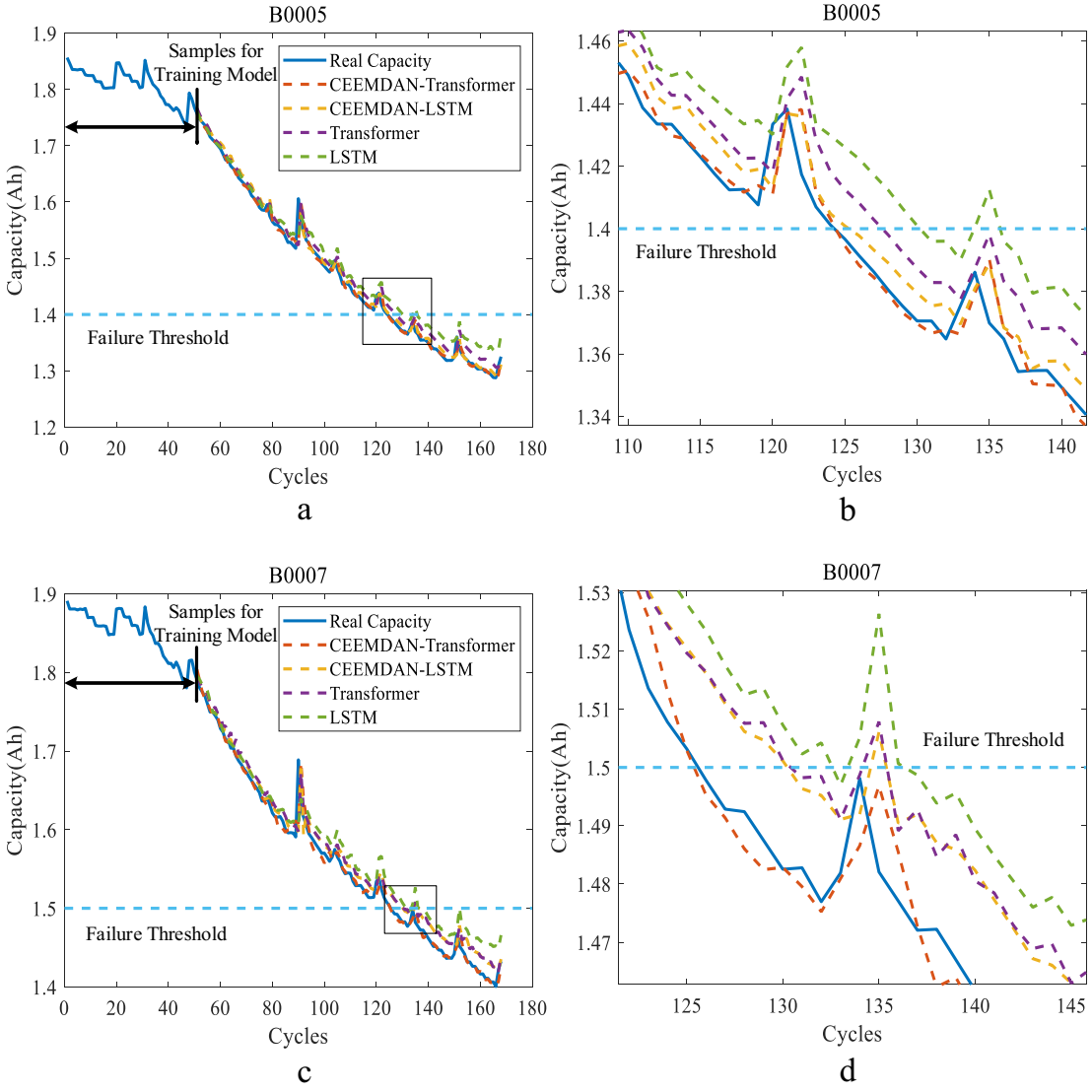

Fig. 6. Predicted curves of batteries B0005 and B0007. a, c, Global view. b, d, Partial enlarged view.

Although the Transformer model's prediction accuracy is better than that of LSTM, the predicted RUL still deviates from the true value. The RMSE value for the CEEMDAN-LSTM combination model is 0.0129, which is lower than that of the solo-LSTM and solo-Transformer models. Furthermore, its predicted RUL result is only one cycle away from the actual RUL, which is superior to the solo models. The proposed model provides more accurate evaluation results, with the predicted RUL matching the actual RUL. The proposed method is more effective than other models in learning battery aging characteristics.

Fig. 6c and d shows the RUL forecasting results for battery B0007. At the 126th cycle, B0007's measured capacity falls below EOL. For LSTM, the battery RUL prediction result is 133, with the Error and PError remaining unsatisfactory at 7 cycles and 5.56 %, respectively. The Transformer's prediction accuracy is higher than that of the LSTM, resulting in a prediction error of five cycles (3.97 %). Furthermore, the Transformer's MAE, MAPE, and RMSE are lower than those of LSTM, indicating that the Transformer outperforms LSTM in terms of battery RUL prediction. The predicted RUL for CEEMDAN-LSTM is 131, and the RMSE, MAE, and MAPE are 0.0175 Ah, 0.0141 Ah, and 0.92 %, respectively. Compared to previous standard models, the proposed model achieves zero prediction deviation from the measured values, and the predicted battery capacity data curves are highly consistent with the measured degradation data.

In order to investigate the feasibility of the proposed method in long-term forecasting, we selected CS2-35 and CS2-37 batteries that had undergone long-term charging and discharging. Fig. 7 shows the measured and predicted capacity curves for these batteries. The measured capacity of CS2-35 decreases below EOL at the 643rd cycle,

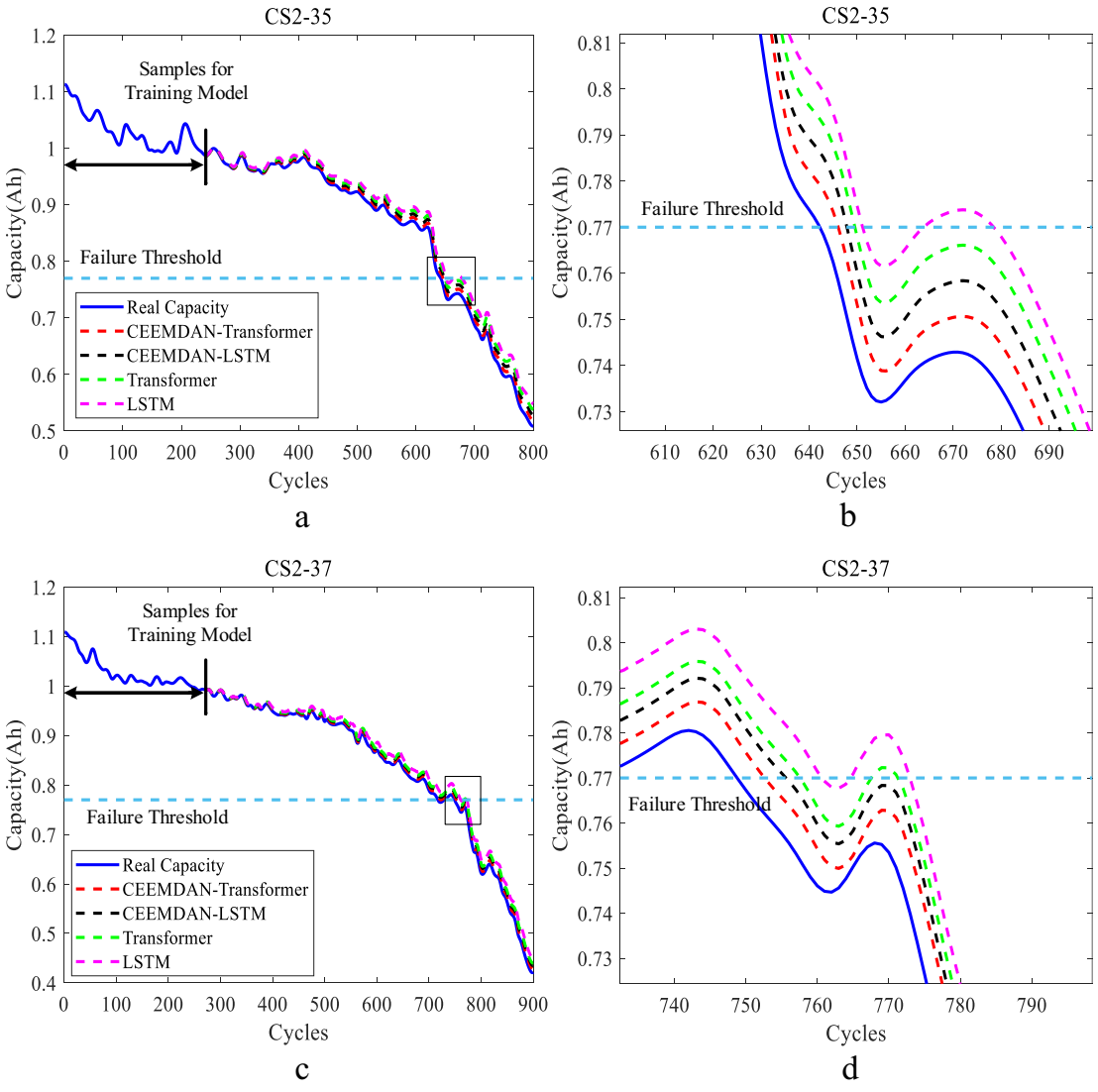

Fig. 7. Predicted curves of batteries CS2-35 and CS2-37. a, c, Global view. b, d, Partial enlarged view.

Table 6
Prediction results of battery CS2–35.

Method	RMSE(Ah)	MAE(Ah)	MAPE	RUL	PRUL	Error	PError
LSTM	0.0241	0.0208	2.79 %	643	652	9	1.40 %
Transformer	0.0185	0.0159	2.13 %	643	650	7	1.09 %
CEEMDAN-LSTM	0.0127	0.0109	1.46 %	643	648	5	0.78 %
CEEMDAN-Transformer	**0.0071**	**0.0060**	**0.80 %**	**643**	**647**	**4**	**0.62 %**

Table 7
Prediction results of battery CS2-37.

Method	RMSE(Ah)	MAE(Ah)	MAPE	RUL	PRUL	Error	PError
LSTM	0.0185	0.0159	2.24 %	749	761	12	1.60 %
Transformer	0.0129	0.0110	1.55 %	749	758	9	1.20 %
CEEMDAN-LSTM	0.0100	0.0084	1.19 %	749	756	7	0.93 %
CEEMDAN-Transformer	**0.0061**	**0.0050**	**0.71 %**	**749**	**753**	**4**	**0.53 %**

while that of CS2-37 drops at the 749th cycle. When comparing the predicted capacity curves to the measured curve, the proposed method's curve shows the strongest match, whereas LSTM's predicted curve is the most distant from the measured curve. The RUL prediction results of various methods are shown in Tables 6 and 7. The combined models achieve better prediction accuracy than the solo models. However, the prediction performance of the solo models degrades significantly due to the influence of the CR. Thus, leveraging the decomposition algorithm enables an enhancement in prediction performance. The proposed method outperforms other methods in terms of its accuracy in predicting

Table 8
Prediction performance of NASA datasets.

	B0005	B0006	B0007	B0018
EOL(Ah)	1.4	1.4	1.5	1.4
ST	51	51	51	40
RUL	125	109	126	95
PRUL	125	110	126	95
RMSE(Ah)	0.0109	0.0174	0.0116	0.0122
MAE(Ah)	0.0060	0.0097	0.0063	0.0095
MAPE	0.41 %	0.68 %	0.40 %	0.64 %
Error	0	1	0	0
PError	0	0.92 %	0	0

Table 9
Prediction performance of CALCE datasets.

	CS2-35	CS2-36	CS2-37	CS2-38
EOL(Ah)	0.77	0.77	0.77	0.77
ST	241	241	271	271
RUL	643	683	749	758
PRUL	647	687	753	760
RMSE(Ah)	0.0071	0.0072	0.0061	0.0077
MAE(Ah)	0.0060	0.0062	0.0050	0.0065
MAPE	0.80 %	0.84 %	0.71 %	0.87 %
Error	4	4	4	2
PError	0.62 %	0.59 %	0.53 %	0.26 %

the RUL of batteries. Specifically, the proposed method yields an Error of four cycles for both CS2-35 and CS2-37. This is the smallest error observed among all methods tested, indicating the superior accuracy of the proposed model in predicting RUL.

4.2. Model online validation

The remaining batteries of NASA and CALCE are used to validate the online prediction performance of the proposed method. The well-trained models are updated with 30 % of actual battery capacity data and then used to forecast future capacity data and RUL using the remaining 70 % data. Tables 8 and 9 show the evaluation results of the RUL prediction for all batteries using the proposed method.

Battery B0006's measured capacity falls below the EOL at the 109th cycle. The proposed models are updated using decomposed capacity data from the first 50 cycles, which represent approximately 30 % of the dataset. Fig. 8a depicts the capacity and RUL prediction results, which demonstrate that the well-trained model achieves an error of only one cycle longer than the real RUL. The RMSE, MAE, and MAPE of the test results are 0.0174 Ah, 0.0097 Ah, and 0.68 %, respectively.

Fig. 8b depicts the predicted results of battery B0018. At the 95th cycle, the true failure threshold is reached, and the predicted capacity also falls below the failure threshold, which corresponds to the actual RUL value. The RMSE, MAE, and MAPE are calculated to be 0.0122 Ah, 0.0095 Ah, and 0.64 %, respectively. These results demonstrate that the well-trained model can accurately predict online RUL without requiring retraining.

Fig. 8c shows the battery prediction results for battery CS2–36 using well-trained models. Only capacity data from the first 30 % of standard discharge experiments are provided to update the trained prediction model. Nonetheless, the proposed method produces outstanding forecasting results. After 687 cycles, the estimated capacity reaches the failure threshold, which is 4 cycles longer than the actual RUL. The calculated RMSE, MAE, and MAPE are 0.0072 Ah, 0.0062 Ah, and 0.84 %, respectively. Similarly, Fig. 8d shows that the proposed model accurately captures the degradation curves for battery CS2–38, with zero error when compared to the actual RUL. The RMSE, MAE, and MAPE of the results are as low as 0.0077 Ah, 0.0065 Ah, and 0.87 %, respectively. These results demonstrate that the proposed method can produce highly accurate online RUL prediction.

4.3. Time cost analysis

A time cost comparison experiment is conducted on the RNN-based models and the Transformer using the batteries B0005 and CS2-35 datasets. The results of Error and RMSE are displayed in Table 10. As shown in Fig. 9, the training time for LSTM and GRU is significantly longer due to their recurrent modeling on sequences, which may require more training time. RNN and Transformer have similar time costs, but the proposed model consistently produces better results due to the multi-head AM used in the model. The Transformer model learns important features in parallel, which accelerates the training process and saves time. In conclusion, the Transformer model obtains good results in terms of prediction accuracy and network training speed.

4.4. Comparison with other advanced methods

To further validate the proposed model's performance, its predicted results are compared with those of models in existing studies that use the same battery aging datasets. To ensure a fair comparison, the prediction ST for all comparison models is kept close to that of the proposed model. Based on NASA datasets, the proposed method has been compared to the following methods: PA-LSTM [32], ARIMA-LSTM [33], ABC-SVR [34] and AUKF-GA-SVR [35]. The RUL prediction results are presented in Table 11, indicating that the proposed method outperforms other advanced methods, as evidenced by its smaller Error. Using B0006 as example, the Error of the proposed method is equal to one cycle, whereas the ARIMA-LSTM and ABC-SVR have Errors of six cycles and four cycles, respectively, which exceed that of the proposed method. The multi-head AM of the Transformer allows the model to efficiently capture important information, making it possible to obtain accurate RUL prediction results even with limited training data.

For CALCE datasets, the proposed method has been compared to several other methods, including: SDDL [31], CEEMDAN-BiGRU-AM [37], EMD-BiGRU-AM [37], NAR [38], EMD-LSTM-GPR [39], DE-WLSSVM-LSTM [40], BMA-LSTMN [41], and NN-BAT-PF [42]. The literature on utilizing the discharge capacity of CALCE batteries as an input feature and predictive variable is limited. So, we relied on existing literature that predicted the SOH to conduct a comparative analysis. The prediction of SOH can yield results for forecasting the RUL as well. Table 12 presents a summary of the comparison between the prediction results of the proposed method and those of other methods. The comparison results show that the proposed method exhibits higher accuracy in RUL prediction compared to most methods in other studies. Therefore, the proposed method is effective in capturing and modeling the complex relationships between battery aging data, resulting in accurate and reliable prediction of RUL.

5. Conclusion

This paper presents a novel battery RUL prediction method based on CEEMDAN and Transformer. The accuracy and reliability of RUL prediction are improved by addressing the CR phenomenon and handling the long-range dependency of capacity fading data with Transformer's multi-head AM. Some conclusions of this paper can be summarized as follows:

1. The proposed method considers the CR phenomenon and decomposes the raw capacity sequence into short-term fluctuations and one long-term residual using the CEEMDAN algorithm. Compared to the solo models, the prediction results of the combined models have lower RMSE and Error. Therefore, the use of decomposition algorithm facilitates the improvement of prediction performance.
2. Transformer-based network is used to model capacity fading data and estimate the battery RUL. The simulation results show that the Transformer can effectively capture both short-term and long-term dependencies in sequential data. Transformer's multi-head AM

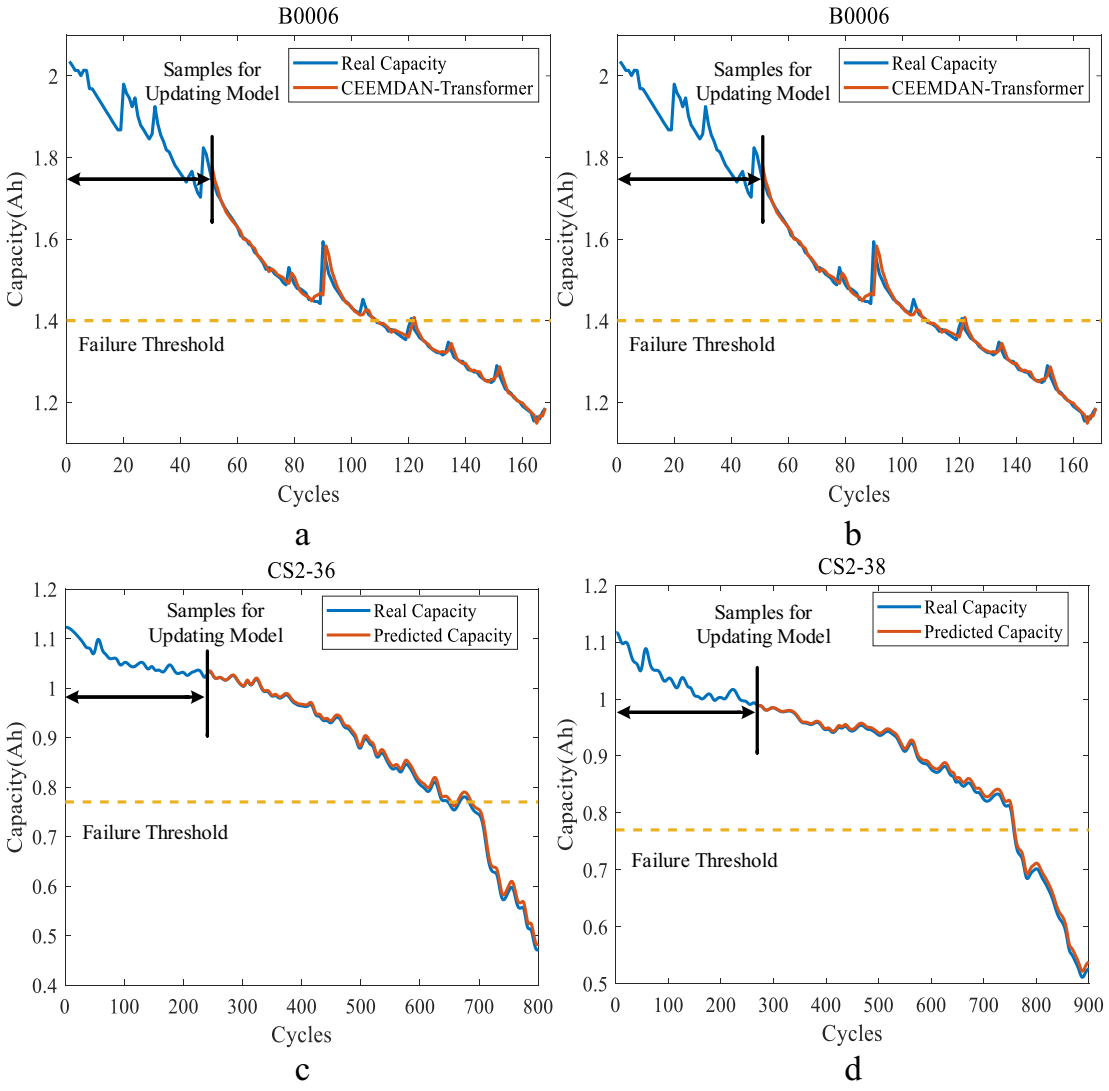

Fig. 8. Online predicted curves of NASA and CALCE datasets. a, battery B0006. b, battery B0018. c, battery CS2-36, d, battery CS2-38.

Table 10
Prediction results of batteries B0005 and CS2-35 based on time cost analysis.

Battery	Method	Error	RMSE
B0005	RNN	8	0.0413
	GRU	6	0.0273
	LSTM	6	0.0262
	Transformer	3	0.0173
CS2-35	RNN	12	0.0423
	GRU	10	0.0276
	LSTM	9	0.0241
	Transformer	7	0.0185

enables it to capture relevant features more efficiently and process input sequences in parallel, thereby reducing the required training data and accelerating model training.

3. The proposed method is developed, tested, and compared to other methods on two publicly available battery aging datasets. The results prove the effectiveness of the proposed method, as it outperforms several advanced approaches of the latest studies, achieving better prediction results while using less training data. Furthermore, the proposed method maintains advantages over RNN based networks in both prediction accuracy and training time.

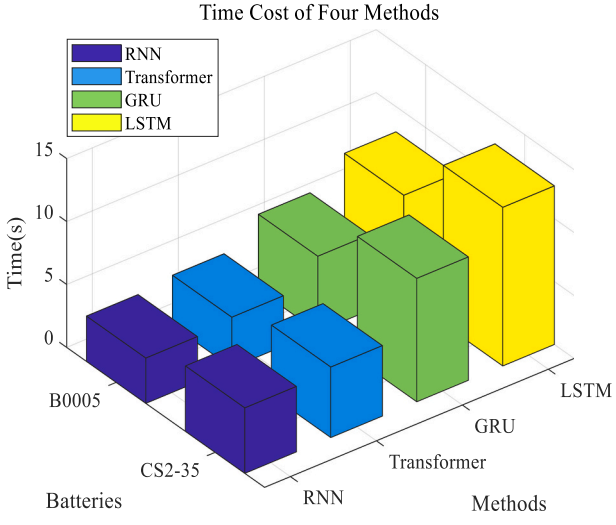

Fig. 9. Time cost of different methods on NASA and CALCE datasets.

In the future, we will study the RUL prediction of lithium-ion

Table 11
Prediction results of NASA datasets on various methods.

Battery	Method	ST	Error
B0005	PA-LSTM [32]	90	3
	ARIMA-LSTM [33]	76	1
	ABC-SVR [34]	84	0
	AUKF-GA-SVR [35]	80	3
	CEEMDAN-Transformer	51	0
B0006	PA-LSTM	90	11
	ARIMA-LSTM	76	6
	ABC-SVR	84	4
	AUKF-GA-SVR	80	16
	CEEMDAN-Transformer	51	1
B0007	ARIMA-LSTM	92	1
	AUKF-GA-SVR	80	0
	CEEMDAN-Transformer	51	0
B0018	PA-LSTM	70	8
	ARIMA-LSTM	59	1
	ABC-SVR	66	0
	AUKF-GA-SVR	60	4
	CEEMDAN-Transformer	40	0

Table 12
Prediction results of CALCE datasets on various methods.

Battery	Method	ST	Error
CS2-35	SDDL [31]	301	5
	CEEMDAN-BiGRU-AM [37]	201	5
	CEEMDAN-BiGRU-AM [37]	301	2
	EMD-BiGRU-AM [37]	301	5
	CEEMDAN-Transformer	241	4
CS2-36	CEEMDAN-BiGRU-AM	201	8
	CEEMDAN-BiGRU-AM	301	4
	EMD-BiGRU-AM	301	7
	NAR [38]	201	5
	EMD-LSTM-GPR [39]	321	6
	DE-WLSSVM-LSTM [40]	283	10
	CEEMDAN-Transformer	241	4
CS2-37	CEEMDAN-BiGRU-AM	201	6
	CEEMDAN-BiGRU-AM	301	2
	EMD-BiGRU-AM	301	5
	NAR	201	6
	DE-WLSSVM-LSTM	195	5
	BMA-LSTMN [41]	301	15
	NN-BAT-PF [42]	301	51
	CEEMDAN-Transformer	271	4
CS2-38	CEEMDAN-BiGRU-AM	201	6
	CEEMDAN-BiGRU-AM	301	3
	EMD-BiGRU-AM	301	8
	CEEMDAN-Transformer	271	2

batteries across diverse operating conditions. This involves collecting and analyzing battery datasets that have been exposed to varying temperatures, currents, and other operational factors. By doing so, we can gain insights into how these factors impact battery performance and develop models that can accurately predict the RUL of batteries operating under different conditions. Moreover, we intend to enhance the prediction ability of the Transformer model by introducing gating mechanisms, increasing depth and width, and using fine-tuning techniques. These efforts will make our method more applicable to real-world applications.

CRediT authorship contribution statement

Zili Wang: Conceptualization, Methodology, Investigation, Data curation, Writing – original draft. **Yonglu Liu:** Conceptualization, Investigation, Validation, Supervision, Funding acquisition. **Fen Wang:** Conceptualization, Methodology, Visualization, Writing – review & editing. **Hui Wang:** Formal analysis, Writing – review & editing. **Mei Su:** Writing – review & editing, Supervision.

Declaration of competing interest

The authors declare that they have no known competing financial interests or personal relationships that could have appeared to influence the work reported in this paper.

Data availability

Data will be made available on request.

Acknowledgements

This paper is supported by the Changsha City Science and Technology Plan Project under Grant kq2009007, and the Innovation-Driven Plan in Central South University under Grant 2023CXQD020.

References

[1] B. Scrosati, J. Hassoun, Y.-K. Sun, Lithium-ion batteries. A look into the future, Energy Environ. Sci. 4 (2011) 3287–3295.
[2] M.-F. Ge, Y. Liu, X. Jiang, J. Liu, A review on state of health estimations and remaining useful life prognostics of lithium-ion batteries, Meas.: J. Int. Meas. Confed. 174 (2021), 109057.
[3] X. Hu, L. Xu, X. Lin, M. Pecht, Battery lifetime prognostics, Joule 4 (2020) 310–346.
[4] X. Hu, D. Cao, B. Egardt, Condition monitoring in advanced battery management systems: moving horizon estimation using a reduced electrochemical model, IEEE/ASME Trans. Mechatron. 23 (2018) 167–178.
[5] A. Guha, A. Patra, Online estimation of the electrochemical impedance spectrum and remaining useful life of lithium-ion batteries, IEEE Trans. Instrum. Meas. 67 (2018) 1836–1849.
[6] Y.H. Lui, M. Li, A. Downey, S. Shen, V.P. Nemani, H. Ye, C. VanElzen, G. Jain, S. Hu, S. Laflamme, C. Hu, Physics-based prognostics of implantable-grade lithium-ion battery for remaining useful life prediction, J. Power Sources 485 (2021), 229327.
[7] W. Waag, C. Fleischer, D.U. Sauer, Critical review of the methods for monitoring of lithium-ion batteries in electric and hybrid vehicles, J. Power Sources 258 (2014) 321–339.
[8] C. Chen, M. Pecht, Prognostics of lithium-ion batteries using model-based and data-driven methods, in: Proceedings of the IEEE 2012 Prognostics and System Health Management Conference (PHM-2012 Beijing), IEEE, 2012, pp. 1–6.
[9] Z. Liu, G. Sun, S. Bu, J. Han, X. Tang, M. Pecht, Particle learning framework for estimating the remaining useful life of lithium-ion batteries, IEEE Trans. Instrum. Meas. 66 (2017) 280–293.
[10] M.A. Patil, P. Tagade, K.S. Hariharan, S.M. Kolake, T. Song, T. Yeo, S. Doo, A novel multistage support vector machine based approach for Li ion battery remaining useful life estimation, Appl. Energy 159 (2015) 285–297.
[11] H. Li, D. Pan, C.L.P. Chen, Intelligent prognostics for battery health monitoring using the mean entropy and relevance vector machine, IEEE Trans. Syst. Man Cybern.: Syst. 44 (2014) 851–862.
[12] Y. Zhang, R. Xiong, H. He, M.G. Pecht, Long short-term memory recurrent neural network for remaining useful life prediction of lithium-ion batteries, IEEE Trans. Veh. Technol. 67 (2018) 5695–5705.
[13] R.R. Richardson, M.A. Osborne, D.A. Howey, Gaussian process regression for forecasting battery state of health, J. Power Sources 357 (2017) 209–219.
[14] M.E. Orchard, L. Tang, B. Saha, K. Goebel, G. Vachtsevanos, Risk-sensitive particle-filtering-based prognosis framework for estimation of remaining useful life in energy storage devices, Stud. Inform. Control. 19 (2010) 209–218.
[15] Y. Zhou, M. Huang, Lithium-ion batteries remaining useful life prediction based on a mixture of empirical mode decomposition and ARIMA model, Microelectron. Reliab. 65 (2016) 265–273.
[16] K. Liu, Y. Shang, Q. Ouyang, W.D. Widanage, A data-driven approach with uncertainty quantification for predicting future capacities and remaining useful life of lithium-ion battery, IEEE Trans. Ind. Electron. 68 (2021) 3170–3180.
[17] Y. Mo, Q. Wu, X. Li, B. Huang, Remaining useful life estimation via transformer encoder enhanced by a gated convolutional unit, J. Intell. Manuf. 32 (2021) 1997–2006.
[18] B. Zhou, C. Cheng, G. Ma, Y. Zhang, Remaining useful life prediction of lithium-ion battery based on attention mechanism with positional encoding, IOP Conf. Ser. Mater. Sci. Eng. 895 (2020) 12006.
[19] L. Ren, J. Dong, X. Wang, Z. Meng, L. Zhao, M.J. Deen, A data-driven auto-CNN-LSTM prediction model for lithium-ion battery remaining useful life, IEEE Trans. Industr. Inform. 17 (2021) 3478–3487.
[20] F.-K. Wang, Z.E. Amogne, J.-H. Chou, C. Tseng, Online remaining useful life prediction of lithium-ion batteries using bidirectional long short-term memory with attention mechanism, Energy (Oxford) 254 (2022), 124344.
[21] A. Vaswani, N. Shazeer, N. Parmar, J. Uszkoreit, L. Jones, A.N. Gomez, L. Kaiser, I. Polosukhin, Attention Is all you Need, Cornell University Library, arXiv.org, Ithaca, 2017.
[22] D. Chen, W. Hong, X. Zhou, Transformer network for remaining useful life prediction of Lithium-ion batteries, IEEE Access 10 (2022) 19621–19628.

[23] M.S.H. Lipu, M.A. Hannan, A. Hussain, M.M. Hoque, P.J. Ker, M.H.M. Saad, A. Ayob, A review of state of health and remaining useful life estimation methods for lithium-ion battery in electric vehicles: challenges and recommendations, J. Clean. Prod. 205 (2018) 115–133.
[24] Z. Wu, N.E. Huang, Ensemble empirical mode decomposition: a noise-assisted data analysis method, Adv. Adapt. Data Anal. 01 (2009) 1–41.
[25] J.-R. Yeh, J.-S. Shieh, N.E. Huang, Complementary ensemble empirical mode decomposition: a novel noise enhanced data analysis method, Adv. Adapt. Data Anal. 02 (2010) 135–156.
[26] M.E. Torres, M.A. Colominas, G. Schlotthauer, P. Flandrin, A complete ensemble empirical mode decomposition with adaptive noise, in: 2011 IEEE International Conference on Acoustics, Speech and Signal Processing (ICASSP), 2011, pp. 4144–4147.
[27] K. He, X. Zhang, S. Ren, J. Sun, Deep residual learning for image recognition, in: 2016 IEEE Conference on Computer Vision and Pattern Recognition (CVPR), IEEE, 2016, pp. 770–778.
[28] J. Lei, J.R. Kiros, G.E. Hinton, Layer Normalization, Cornell University Library, arXiv.org, Ithaca, 2016.
[29] B. Saha, K. Goebel, Battery Data Set, NASA AMES Prognostics Data Repository, 2007.
[30] W. He, N. Williard, M. Osterman, M. Pecht, Prognostics of lithium-ion batteries based on Dempster–Shafer theory and the Bayesian Monte Carlo method, J. Power Sources 196 (2011) 10314–10321.
[31] Z. Chen, L. Chen, W. Shen, K. Xu, Remaining useful life prediction of lithium-ion battery via a sequence decomposition and deep learning integrated approach, IEEE Trans. Veh. Technol. 71 (2022) 1466–1479.
[32] J. Qu, F. Liu, Y. Ma, J. Fan, A neural-network-based method for RUL prediction and SOH monitoring of lithium-ion battery, IEEE Access 7 (2019) 87178–87191.
[33] X. Qin, Q. Zhao, H. Zhao, W. Feng, X. Guan, Prognostics of remaining useful life for lithium-ion batteries based on a feature vector selection and relevance vector machine approach, in: 2017 IEEE International Conference on Prognostics and Health Management (ICPHM), IEEE, 2017, pp. 1–6.
[34] Y. Wang, Y. Ni, S. Lu, J. Wang, X. Zhang, Remaining useful life prediction of lithium-ion batteries using support vector regression optimized by artificial bee colony, IEEE Trans. Veh. Technol. 68 (2019) 9543–9553.
[35] Z. Xue, Y. Zhang, C. Cheng, G. Ma, Remaining useful life prediction of lithium-ion batteries with adaptive unscented kalman filter and optimized support vector regression, Neurocomputing (Amsterdam) 376 (2020) 95–102.
[36] Z. Tong, J. Miao, S. Tong, Y. Lu, Early prediction of remaining useful life for lithium-ion batteries based on a hybrid machine learning method, J. Clean. Prod. 317 (2021), 128265.
[37] F. Xia, K. Wang, J. Chen, State of health and remaining useful life prediction of lithium-ion batteries based on a disturbance-free incremental capacity and differential voltage analysis method, J. Energy Storage 64 (2023), 107161.
[38] B. Gou, Y. Xu, X. Feng, State-of-health estimation and remaining-useful-life prediction for lithium-ion battery using a hybrid data-driven method, IEEE Trans. Veh. Technol. 69 (2020) 10854–10867.
[39] H. Pan, C. Chen, M. Gu, A method for predicting the remaining useful life of lithium batteries considering capacity regeneration and random fluctuations, Energies 15 (2022) 2498.
[40] J. Wang, S. Zhang, C. Li, L. Wu, Y. Wang, A data-driven method with mode decomposition mechanism for remaining useful life prediction of lithium-ion batteries, IEEE Trans. Power Electron. 37 (2022) 13684–13695.
[41] Y. Liu, G. Zhao, X. Peng, Deep learning prognostics for lithium-ion battery based on ensembled long short-term memory networks, IEEE Access 7 (2019) 155130–155142.
[42] Y. Wu, W. Li, Y. Wang, K. Zhang, Remaining useful life prediction of lithium-ion batteries using neural network and bat-based particle filter, IEEE Access 7 (2019) 54843–54854.